IFNγ enhances ferroptosis by increasing JAK-STAT pathway activation to suppress SLCA711 expression in adrenocortical carcinoma

XINBO YU[1*], DANDAN ZHU[1*], BIXIAN LUO[2*], WEI KOU[1], YULING CHENG[1] and YU ZHU[1]

Departments of [1]Urology and [2]General Surgery, Ruijin Hospital, Shanghai Jiaotong University School of Medicine, Shanghai 200025, P.R. China

Received November 10, 2021; Accepted March 2, 2022

DOI: 10.3892/or.2022.8308

Abstract. Adrenocortical carcinoma (ACC) is a rare type of tumor with a poor prognosis. Ferroptosis is a relatively novel form of programmed cell death driven by iron-dependent lipid peroxidation accumulation. Recent evidence suggests that IFNγ facilitates erastin-induced ferroptosis, which contributed to anticancer therapy in various types of cancer. However, it has remained elusive whether the regulation of IFNγ on ferroptosis has a positive role in the treatment of ACC. Thus, the aim of the present study was to explore the effects of IFNγ on erastin-induced ferroptosis in the ACC cell line NCI-H295R and investigate the underlying mechanisms. Cell viability was assessed using a Cell Counting Kit-8 assay, an ethynyldioxyuridine proliferation assay and Live/Dead staining. The levels of iron, reactive oxygen species, lipid peroxidation and mitochondrial damage were also assessed. Western blot and reverse transcription-quantitative PCR analyses were used to determine the underlying molecular mechanisms involved in the erastin-induced ferroptosis of NCI-H295R cells. The results suggested that IFNγ promoted erastin-induced ferroptotic cell death. Furthermore, IFNγ enhanced erastin-induced ferroptosis, as evidenced by the accumulation of iron, as well as the increase in lipid peroxidation and promotion of mitochondrial damage. Further analysis suggested that IFNγ enhanced ferroptosis by suppressing the expression of solute carrier family 7 member 11, an important negative regulator of ferroptosis, and this was achieved via activation of the JAK/STAT pathway in NCI-H295R cells. The present study provided experimental evidence on the activity and mechanism of ferroptosis enhanced by IFNγ in ACC and may give critical insight into the immunotherapeutic management of ACC.

Correspondence to: Dr Yu Zhu, Department of Urology, Ruijin Hospital, Shanghai Jiaotong University School of Medicine, 97 2nd Ruijin Road, Shanghai 200025, P.R. China
E-mail: zy10478@rjh.com.cn

*Contributed equally

Key words: adrenocortical carcinoma, IFNγ, SLC7A11, ferroptosis, JAK/STAT pathway

Introduction

Adrenocortical carcinoma (ACC) is rare endocrine neoplasia with an annual incidence rate of 0.7-2 cases/million individuals (1). It is an aggressive cancer type and lacks efficacious therapies. Early diagnosis, complete surgical resection and adjuvant therapy with mitotane are recommended as the curative treatment for ACC (2). Immunotherapy is also feasible and rational in the management of ACC; however, an increasing body of evidence suggests that the clinical efficacy of immunotherapy is modest in patients with ACC (3-5). Productive $CD8^+$ T-cell infiltrates induce antitumor immune responses to promote tumor clearance. TP53 germline mutations and Wnt/β-catenin activation have important roles in ACC tumorigenesis, which result in impaired $CD8^+$ function and immunoresistance (6). Therefore, novel therapeutic strategies are required to overcome immunoresistance in ACC.

IFNγ is an essential cytokine for antitumor immunity and may inhibit tumor growth by inducing cell cycle arrest and apoptosis (7). $CD8^+$ T cells exhibit cytolytic activities involving perforin or the Fas mechanism to achieve tumor clearance (8). $CD8^+$ T cells are the major source of IFNγ production (9,10). Previous studies have indicated that the IFNγ produced by $CD8^+$ T cells appears to improve antitumor responses by enhancing tumor sensitivity to ferroptosis (11,12).

Ferroptosis is an iron-dependent cell death that differs from traditional apoptosis, necrosis and autophagy with regard to both the cellular morphological changes and the and gene expression profiles (13). This relatively recently discovered form of regulated cell death is characterized by lipid peroxidation and accumulation of reactive oxygen species (ROS) (14). Acyl-CoA synthase long chain family member 4 (ACSL4) participates in the synthesis of oxidized cellular membrane phospholipids capable of controlling the sensitivity of cells to ferroptosis (15).

Solute carrier family 7 member 11 (SLC7A11) is an important negative regulator of ferroptosis and encodes the light chain subunit of system Xc-. System Xc- is an amino acid antiporter located in the plasma membrane, which allows for

cystine uptake and glutamate release (16). Once cystine enters cells, it is reduced to cysteine, which in turn is used in the biosynthesis of glutathione (GSH). GSH is the major intracellular antioxidant and cofactor of GSH peroxidase 4 (GPX4), which prevents cells from experiencing oxidative stress and therefore undergoing ferroptosis (17). Erastin is able to inhibit system Xc-activity and subsequently cause GSH depletion, resulting in increased ferroptosis. In addition to killing tumor cells, several studies have demonstrated that erastin enhances the sensitivity of cancers to chemotherapy and radiotherapy (18-20). Previous studies have also indicated that IFNγ facilitates erastin-induced ferroptosis, which contributes to anticancer therapy in various types of cancer (11,12). However, it remains elusive whether the regulatory effect of IFNγ on ferroptosis has a positive role in the therapy of ACC.

In the present study, it was demonstrated that IFNγ promoted erastin-induced ferroptotic cell death. In addition, IFNγ enhanced erastin-induced ferroptosis, as evidenced by the accumulation of iron, elevation of lipid peroxidation and increase in mitochondrial damage. Further analysis indicated that IFNγ enhanced ferroptosis by suppressing the expression of SLC7A11, which was achieved through the activation of the JAK/STAT pathway in NCI-H295R cells. Taken together, these results suggest that targeting SLC7A11 predisposes ACC cells to ferroptosis and this may provide a novel strategy to improve the efficacy of immunotherapy in ACC.

Materials and methods

Identification of prognostic ferroptosis-related differentially expressed genes (DEGs). The RNA sequencing data of 128 normal samples and 79 ACC samples were downloaded from the UCSC Xena platform (https://xena.ucsc.edu/). In addition, the clinical information of 79 patients with ACC was obtained from The Cancer Genome Atlas (TCGA) database (https://portal.gdc.cancer.gov/). A total of 60 ferroptosis-related genes (FRGs) were acquired from previous research (21). All DEGs were analyzed using R (version 4.10) (22). For DEGs, a false discovery rate of <0.05 was used as a cutoff criterion and was processed using the limma R package (23). Univariate Cox analysis was performed using the survival R package, with the aim of evaluating the interaction between FRGs and overall survival (OS). All genes with P<0.001 were considered prognostic genes. The Venn R package was used to draw Venn diagrams and identify the intersection genes between the DEGs and prognostic genes. Next, GEPIA2 (http://gepia2.cancer-pku.cn/#index) was used to perform survival analysis of the intersection genes (24). Overall survival was estimated by Kaplan-Meier analysis, and the P-values were determined by log-rank test. P<0.05 was considered to indicate a statistically significant difference.

Cell culture and drugs. The human ACC cell line NCI-H295R was purchased from Procell Life Science & Technology Co., Ltd. Cells were incubated in DMEM/F12 media with added 6.25 μg/ml insulin, 6.25 μg/ml transferrin, 6.25 ng/ml selenium, 5.35 μg/ml linoleic acid, 10% FBS and 1% penicillin/streptomycin (all from Procell Life Science & Technology Co., Ltd.). Cells were maintained in a humidified incubator supplied with 5% CO_2 at 37˚C. Recombinant human IFNγ (cat. no. HY-P7025A), erastin (cat. no. HY-15763) and fludarabine (cat. no. HY-B0069) were purchased from MedChemExpress. Erastin and fludarabine were dissolved in DMSO and then diluted in complete culture medium to the desired concentration, with a final DMSO concentration of <0.1%.

Cell viability assay. NCI-H295R cells were seeded into a 96-well plate at a density of $1x10^4$ cells/well in 100 μl culture medium. After incubation for 24 h, cells were pretreated with or without IFNγ (10 ng/ml) for 24 h, followed by treatment with erastin (10 or 20 μM) for 24, 48 or 72 h. Cell viability was detected using a Cell Counting Kit-8 (CCK-8) assay (Epizyme Biotech). A total of 10 μl CCK-8 solution was added to each well, followed. By further incubation for 4 h at 37˚C. The optical density value was measured at 450 nm using a plate reader (Tecan infinite F200PRO; Tecan Group, Ltd.) and the percentage of viable cells compared with the control cells was calculated.

Ethynyldioxyuridine (EdU) proliferation assay. An EdU staining assay was performed using an EdU staining kit (Beyotime Institute of Biotechnology) according to the manufacturer's protocol. Cells were stained with 20 μM EdU solution for 4 h and then fixed with fixative solution provided in the staining kit. The cell nuclei were stained with DAPI. The images were acquired using a fluorescence microscope (Eclipse 80i; Nikon Corporation) and stained cells were analyzed using ImageJ software (version 1.53; National Institutes of Health).

Cell death assay. Cell death was detected using a Calcein-acetoxymethyl ester (AM)/propidium iodide (PI) LIVE/DEAD double staining kit (cat. no. CA1630; Beijing Solarbio Science & Technology Co., Ltd.). Cells were harvested and washed using the included Assay Buffer three times. The harvested cells were resuspended in Assay Buffer and subsequently stained with 2 μM calcein-AM (for live cells) and 4.5 μM PI (for dead cells) at 37˚C for 30 min in the dark. Stained cells were imaged using a fluorescence microscope (Eclipse 80i; Nikon Corporation) and analyzed using ImageJ (version 1.53; National Institutes of Health).

Western blot analysis. After treatment, cells were lysed with RIPA lysis buffer supplemented with a protease and phosphatase inhibitor cocktail (Epizyme Biotech). The concentration of the protein samples was quantified using a BCA protein assay kit (Takara Bio, Inc.), total protein (20 μg/lane) was resolved by SDS-PAGE on 10% gels and transferred to PVDF membranes (MilliporeSigma). Membranes were blocked with protein free rapid blocking buffer (Epizyme Biotech) at room temperature for 15 min. Subsequently, the PVDF membrane was incubated with primary antibodies against β-actin (1:1,000 dilution; cat. no. ab8226; Abcam), SLC7A11 (1:1,000 dilution; cat.ARG57998; Arigobio), phosphorylated signal transducer and activator of transcription 1 (p-STAT1; 1:1,000 dilution; cat. no. ab109461; Abcam), STAT1 (1:10,000 dilution; cat. no. ab109320; Abcam) p-STAT3 (1:1,000 dilution; cat. no. ab267373; Abcam), STAT3 (1:1,000 dilution; cat. no. ab68153; Abcam) or IFN regulatory factor 1 (IRF1;

1:1,000 dilution; cat. no. ab243895; Abcam) at 4˚C overnight, followed by horseradish peroxidase (HRP)-labeled secondary antibody (1:1,000 dilution; cat. no. LF101 or LF102; Epizyme Biotech). Protein signals were visualized using Chemiluminescent HRP substrate (MilliporeSigma) and analyzed using ImageJ (version 1.53; National Institutes of Health).

Reverse transcription-quantitative (RT-q) PCR. Total RNA was extracted from cells using Total RNA isolation reagent (Biosharp) and then reverse-transcribed into cDNA using a Takara RT kit (Takara Bio, Inc.). The mixture was incubated at 37˚C for 15 min, followed by 85˚C for 5 sec and then cooled at 4˚C. qPCR was performed using TB Green® Premix Ex Taq™ (Takara Bio, Inc.) in a final volume of 20 μl in an ABI 7500 reactor (Applied Biosystems; Thermo Fisher Scientific, Inc.). The qPCR conditions consisted of an initial denaturation step for 30 sec at 95˚C, followed by 40 cycles of 3 sec denaturation at 95˚C and annealing/elongation for 30 sec at 60˚C. The samples were quantified using the $2^{-\Delta\Delta Cq}$ method and β-actin was used as the internal control (25). The PCR primer sequences (Sangon Biotech, Co., Ltd.) are listed in Table I.

Table I. Primer sequences of genes for quantitative PCR.

Gene	Primer sequence (5'-3')
SLC7A11	
Forward	GGTCCATTACCAGCTTTTGTACG
Reverse	AATGTAGCGTCCAAATGCCAG
GPX4	
Forward	GAGGCAAGACCGAAGTAAACTAC
Reverse	CCGAACTGGTTACACGGGAA
ACSL4	
Forward	CATCCCTGGAGCAGATACTCT
Reverse	TCACTTAGGATTTCCCTGGTCC
β-actin	
Forward	GACCTGTACGCCAACACAGT
Reverse	CTCAGGAGGAGCAATGATCT

SLC7A11, solute carrier family 7 member 11; ACSL4, acyl-CoA synthase long chain family member 4; GPX4, glutathione peroxidase 4.

Immunofluorescence analysis. After treatment, the cells were washed with PBS three times, fixed in 4% formaldehyde for 24 h and blocked with 5% goat serum (cat. no. C0265; Beyotime Institute of Biotechnology) for 60 min. Next, the cells were incubated with the anti-SLC7A11 primary antibody (1:1,000 dilution; cat. ARG57998; Arigobio) at 4˚C overnight. The following day, the cells were washed with PBS and incubated with the secondary antibody (donkey anti-rabbit IgG H&L; 1:1,000 dilution; cat. no. ab150075; Abcam) for 2 h at room temperature, and the nuclei were stained with DAPI. Finally, the fluorescently labeled cells were visualized using fluorescence microscopy (Eclipse 80i; Nikon Corporation).

Lipid peroxidation detection using BODIPY-C11. Lipid peroxidation was detected using a C11 BODIPY 581/591 probe (ABclonal Biotech Co., Ltd.). Cells were incubated with 50 μM working solution for 1 h at 37˚C and gently washed with PBS three times. Finally, cells were imaged using a fluorescence microscope (Eclipse 80i; Nikon Corporation).

Measurement of intracellular iron levels. For assaying of intracellular iron levels, Phen Green SK (PGSK), a fluorescent probe (Cayman Chemical Company), was used. Cells were incubated with 50 μM PGSK at 37˚C for 20 min and then the fluorescence images were acquired. Finally, the intensity of green fluorescence was measured using ImageJ (version 1.53; National Institutes of Health).

Transmission electron microscopy. After treatment, cells were harvested and fixed in 2.5% glutaraldehyde at 4˚C for 12 h. The samples were rinsed, dehydrated in a gradient series of alcohol solutions, embedded and sectioned (70-90 nm). The sections were stained using uranyl acetate/lead citrate for 10 min prior to observation. Morphological changes in the mitochondria were imaged using a transmission electron microscope (H-7650; Hitachi, Ltd.). The mitochondrial area and density were quantitatively analyzed by ImageJ software (version 1.53; National Institutes of Health).

Detection of intracellular ROS. Intracellular ROS was measured using an ROS assay kit (Beyotime Institute of Biotechnology) according to the manufacturer's protocol. In brief, after treatment, cells were incubated with 10 μM dichloro-dihydro-fluorescein diacetate probe at 37˚C for 20 min. The fluorescent cells were observed using a fluorescence microscope and the intracellular ROS levels were detected using a flow cytometer (CytoFlex S; Beckman Coulter, Inc.).

Detection of mitochondrial membrane potential (MMP). The JC-1 fluorescent probe (MMP assay kit with JC-1; no. C2006; Beyotime Institute of Biotechnology) was used to evaluate the MMP of cells according to the manufacturer's protocol. When the MMP is high, JC-1 accumulates in the matrix of the mitochondria to form a polymer (J-aggregates), which fluoresces red; when the MMP is low, JC-1 does not aggregate in the mitochondrial matrix but is present as a monomer and fluoresces green. Thus, it is convenient to detect the changes in MMP based on the change in fluorescence color. The relative ratio of red to green fluorescence may be used to measure mitochondrial depolarization. NCI-H295R cells were seeded into 6-well plates at a density of $2x10^5$ cells/well. Cells were pretreated with or without IFN-γ (10 ng/ml) for 24 h, followed by treatment with erastin (20 μM) for 48 h. Cells were washed with PBS and stained with 1 ml of the JC-1 staining solution per ml of culture medium added to each well of the plate, with incubation at 37˚C for 20 min. The supernatant was then discarded and the cells were washed two times with JC-1 staining buffer. The fluorescence images were then obtained using a fluorescence microscope (Eclipse 80i; Nikon Corporation) in 6 random fields under a magnification of x400. ImageJ software (version 1.53; National Institutes of Health) was used to measure the fluorescence intensity.

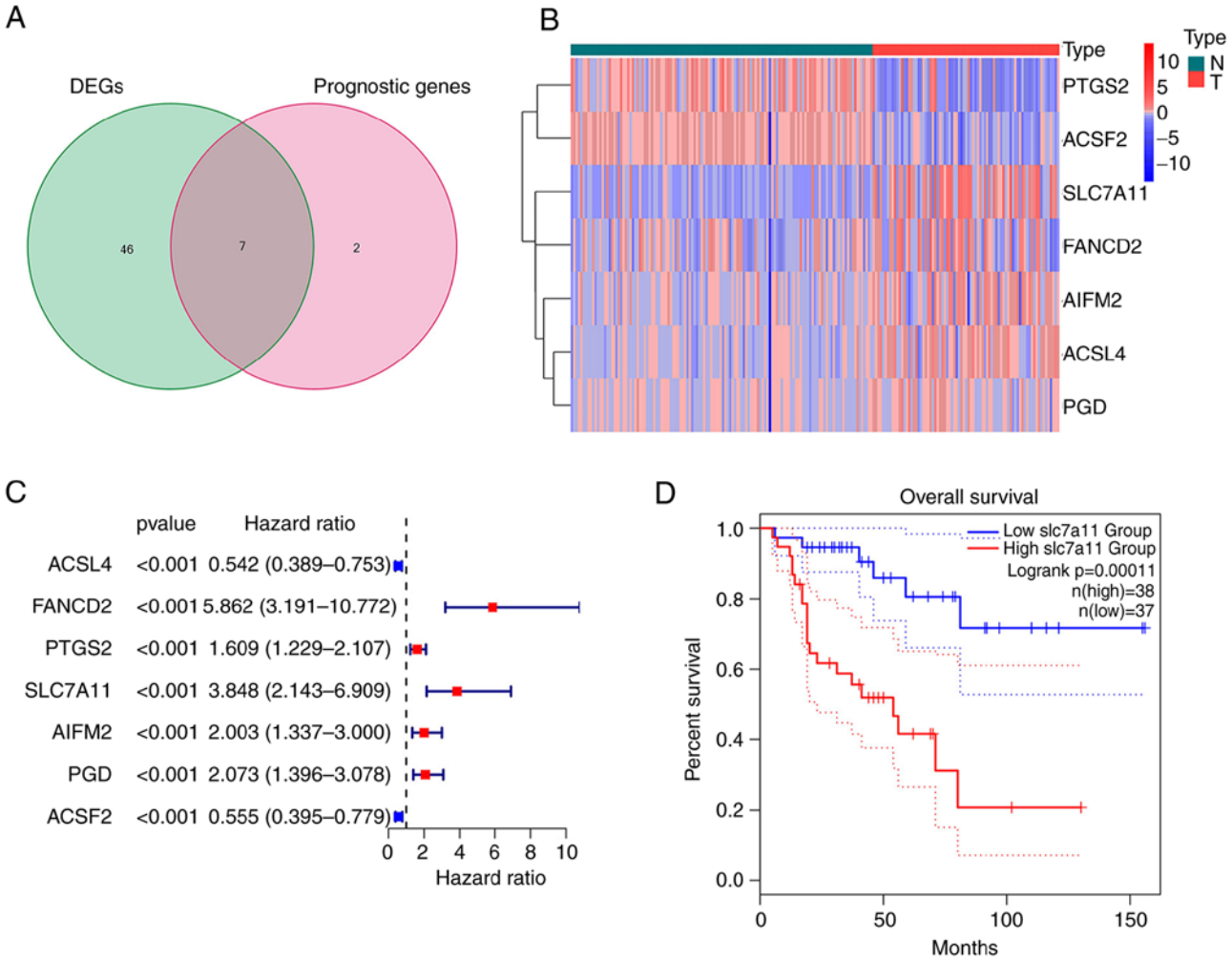

Figure 1. Extraction of ferroptosis-related gene in ACC. (A) Venn diagram displaying the seven ferroptosis-related prognostic DEGs. (B) Downregulated and upregulated intersection genes are presented in a heatmap. (C) Univariate regression forest plot of 7 intersection genes. (D) Kaplan-Meier survival curve of SLC7A11 in patients with ACC. DEG, differentially expressed gene; SLC7A11, solute carrier family 7 member 11; T, tumor sample; N, normal control; ACC, adrenocortical carcinoma.

Overexpression of SLC7A11 and suppression of STAT1. pCMV-SLC7A11-ZsGreen-PURO and pcDNA3.1-ZsGreen-PURO plasmids were purchased from Hanbio Biotechnology Co., Ltd. The plasmid was transfected into NCI-H295R cells to overexpress SLC7A11, while the mock plasmid was used as the negative control. Cells were seeded in a six-well plate ($2x10^5$ cells/well) and grown to 60-70% confluence at 37˚C with 5% CO_2 prior to transfection. Transfection was performed using Lipofectamine® 3000 reagent (Invitrogen; Themo Fisher Scientific, Inc.) and Ultra-MEM Reduced Serum Medium (BioAgrio) for 6 h at 37˚C with 5% CO_2. The medium was then replaced with supplemented culture medium for a further 18 h. Subsequently, cells were treated with IFNγ (10 ng/ml) for 24 h, followed by erastin (20 μM) for 48 h. The efficacy of overexpression was analyzed by RT-qPCR and western blot analysis.

Fludarabine was used to inhibit the expression of STAT1. Cells were seeded in a six-well plate ($2x10^5$ cells/well) at 37˚C with 5% CO_2 overnight; after 24 h pre-treatment with 2 μM fludarabine at 37˚C, NCI-H295R cells were treated with IFNγ (10 ng/ml) for 24 h, followed by erastin (20 μM) for 48 h.

Statistical analysis. Values are expressed as the mean ± standard deviation of three or more independent experiments. Student's t-test was used to analyze the differences between two groups. Comparisons among multiple groups were performed using a one-way ANOVA followed by a Tukey's post-hoc test. Statistical analyses were performed using the NCSS statistical software version 21.0.3 (NCSS, LLC). $P<0.05$ was considered to indicate a statistically significant difference.

Results

Extraction of FRGs in ACC. The majority of the FRGs (53/60, 88.33%) were differentially expressed between the ACC and normal adrenal gland tissues. Of these, 7 were identified as prognostic factors based on the univariate Cox regression analysis ($P<0.001$; Fig. 1A). These intersection genes were further evaluated using a heatmap and univariate Cox regression analysis. The heatmap presents the expression levels of FRGs between normal and tumor tissues; downregulated genes are indicated with blue squares and upregulated genes with red squares (Fig. 1B). Analysis of the relationship between FRGs and OS was visualized using a forest plot (Fig. 1C). The results suggested that

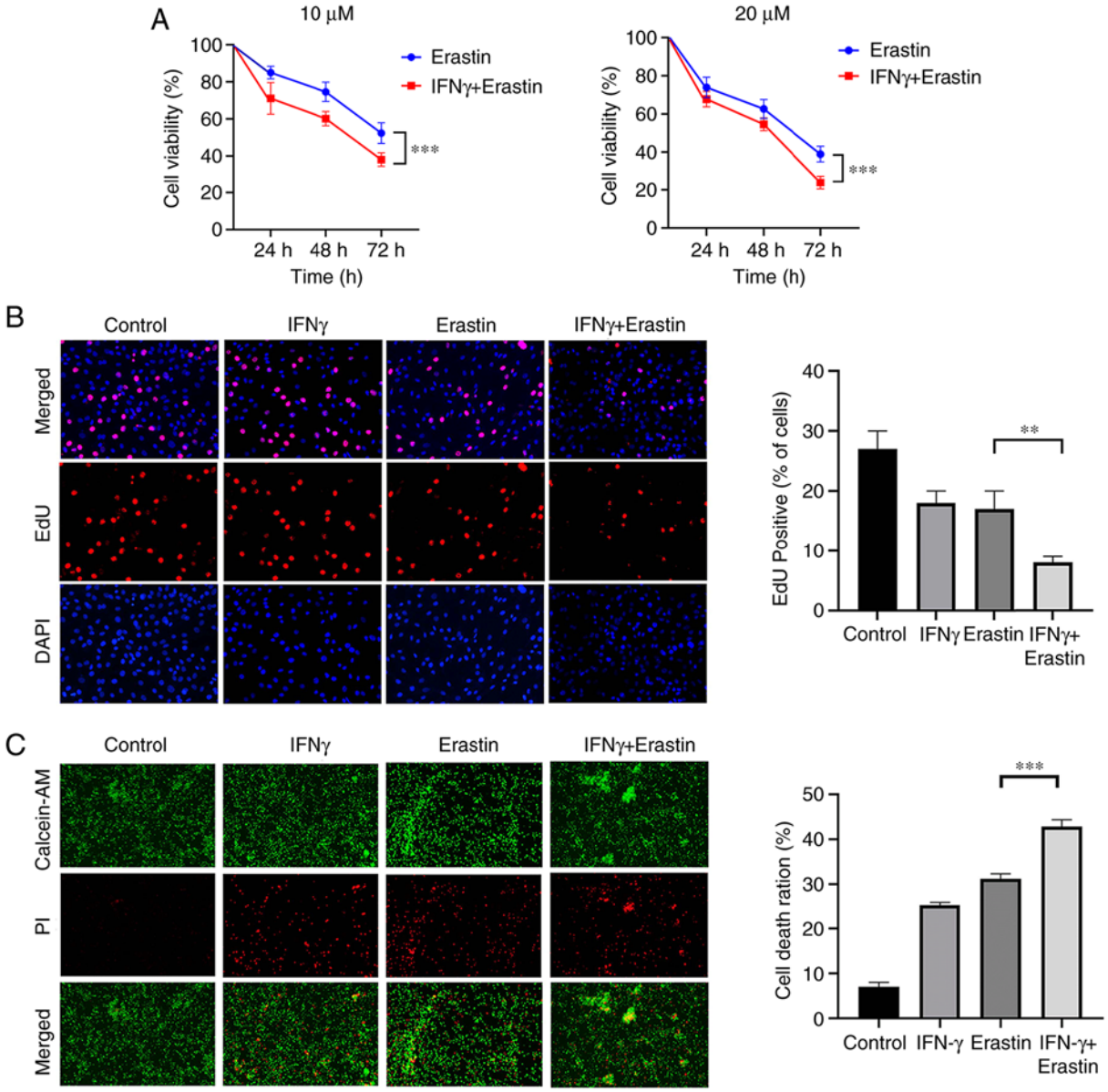

Figure 2. IFNγ sensitizes NCI-H295R cells to ferroptotic cell death. (A) Cell viability was detected by a Cell Counting Kit-8 assay and presented as a percentage of the control (n=6). (B) EdU staining assay was performed to determine cell proliferation (magnification, x400). (C) NCI-H295R cell death was analyzed with a LIVE/DEAD Cell Imaging Kit (magnification, x100). Values are expressed as the mean ± standard deviation (**P<0.01 and ***P<0.001). EdU, ethynyldioxyuridine; PI, propidium iodide; AM, acetoxymethyl ester.

SLC7A11 was upregulated in patients with ACC and its high expression was related to poor survival. Kaplan-Meier curves suggested that low expression of SLC7A11 in patients with ACC was associated with a favorable prognosis (Fig. 1D). The results of the Kaplan-Meier curve analysis for the other intersection genes [Fanconi anemia group D2 protein (FANCD2); apoptosis inducing factor mitochondria associated 2 (AIFM2); phosphogluconate dehydrogenase (PGD); ACSL4; acyl-CoA synthetase family member 2 (ACSF2); prostaglandin-endoperoxide synthase 2 (PTGS2)] are provided in Fig. S1; these findings demonstrated that the expression of other intersection genes was associated with the prognosis of patients with ACC (P<0.05).

IFNγ sensitizes NCI-H295R cells to ferroptotic cell death. NCI-H295R cells were treated with 10 ng/ml IFNγ for 24 h, followed by treatment with different concentrations of erastin for 24, 48 and 72 h. To analyze the viability of NCI-H295R cells, a CCK-8 assay was performed. The results indicated that erastin exerted a dose- and time-dependent inhibitory effect on the viability of NCI-H295R cells compared with the control group. Pretreatment of IFNγ further enhanced the inhibitory effect of erastin on NCI-H295R cell viability (Fig. 2A). The EdU assay suggested that the percentage of EdU-positive cells was decreased by erastin treatment and this was attenuated by IFNγ pretreatment (Fig. 2B). Live/Dead assay staining further confirmed the cytotoxic effect of the above-mentioned treatment. Green fluorescence represents live cells and red fluorescence represents dead cells. The combination of IFNγ and erastin resulted in a higher cell death ratio compared with cells treated with erastin alone (Fig. 2C). All of these results indicated that IFNγ sensitized NCI-H295R cells to erastin-induced cell death.

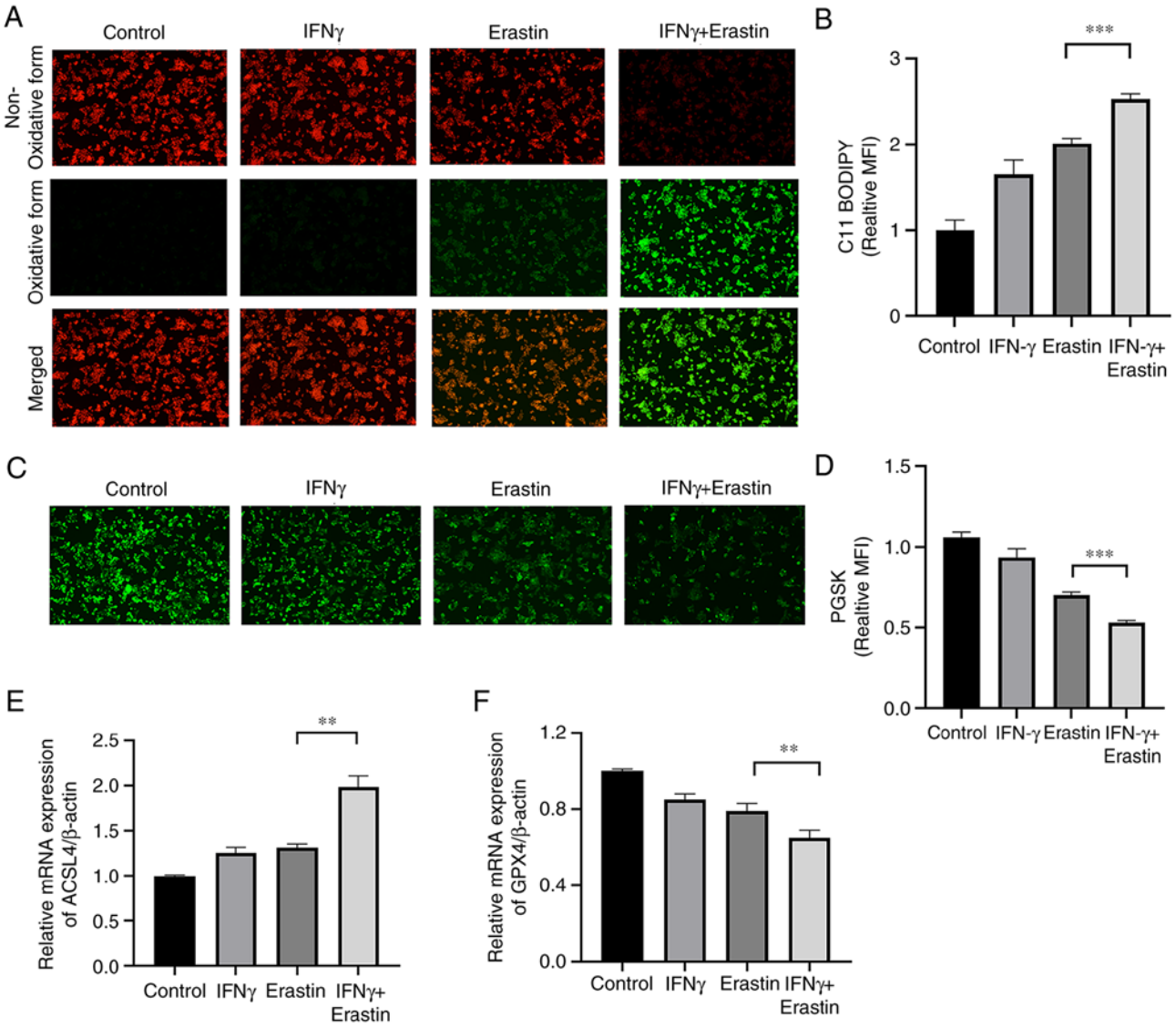

Figure 3. IFNγ enhances erastin-induced ferroptosis. (A) Lipid peroxidation was assessed by C11-BODIPY; red fluorescence represents the non-oxidized form, while green fluorescence represents the oxidized form (magnification, x100). (B) Bar graph presenting the green MFI from A (n=3). (C) Representative images of PGSK staining obtained by a fluorescence microscope (magnification, x100). (D) Bar graph displaying the relative iron content (n=3). (E and F) Reverse transcription-quantitative PCR analysis of the expression of ACSL4 and GPX4 (n=3). Values are expressed as the mean ± standard deviation (**P<0.01 and ***P<0.001). PGSK, Phen Green SK; ACSL4, acyl-CoA synthase long chain family member 4; MFI, mean fluorescence intensity; GPX4, glutathione peroxidase.

IFNγ enhances erastin-induced ferroptosis. To determine whether IFNγ enhanced the sensitivity of NCI-H295R cells to erastin, the levels of lipid peroxidation and intracellular iron were assessed. The C11-BODIPY581/591 fluorescence probe is a lipid peroxidation sensor, capable of accessing the cell membrane. Once oxidized, the fluorescent properties shift from a non-oxidative form (red fluorescence) to an oxidative form (green fluorescence). The results suggested that IFNγ pretreatment accelerated the process of decay of red fluorescence to green fluorescence (Fig. 3A and B). The intracellular iron content may quench PGSK fluorescence. The fluorescence intensity of the PGSK probe was decreased in the IFNγ + erastin group, indicative of an accumulation of iron (Fig. 3C and D). Both ACSL4 and GPX4 are important indicators of ferroptosis. The RT-qPCR assay indicated increased mRNA levels of ACSL4 and decreased mRNA levels of GPX4 in the IFNγ + erastin group compared with the control group (Fig. 3E and F).

Mitochondrial damage caused by erastin-induced ferroptosis is enhanced by IFNγ. The mitochondria are the primary sites of ROS production, and ROS has important roles in ferroptosis. Therefore, the impact of IFNγ on mitochondrial damage in erastin-treated cells was further analyzed. MMP assays indicated an increased green/red fluorescence ratio and loss of MMP in the erastin-treated cells after pretreatment with IFNγ (Fig. 4A and B). Furthermore, fluorescence microscopy and flow cytometric analysis suggested that IFNγ enhanced intracellular ROS generation in the NCI-H295R cells followed by treatment with erastin (Fig. 4C-F). In addition, the morphology of the mitochondria in the NCI-H295R cells was observed using transmission electron microscopy. Upon exposure to IFNγ and erastin, the mitochondria became smaller, the membrane density increased and the area of ruptured membrane also increased (Fig. 4G-I).

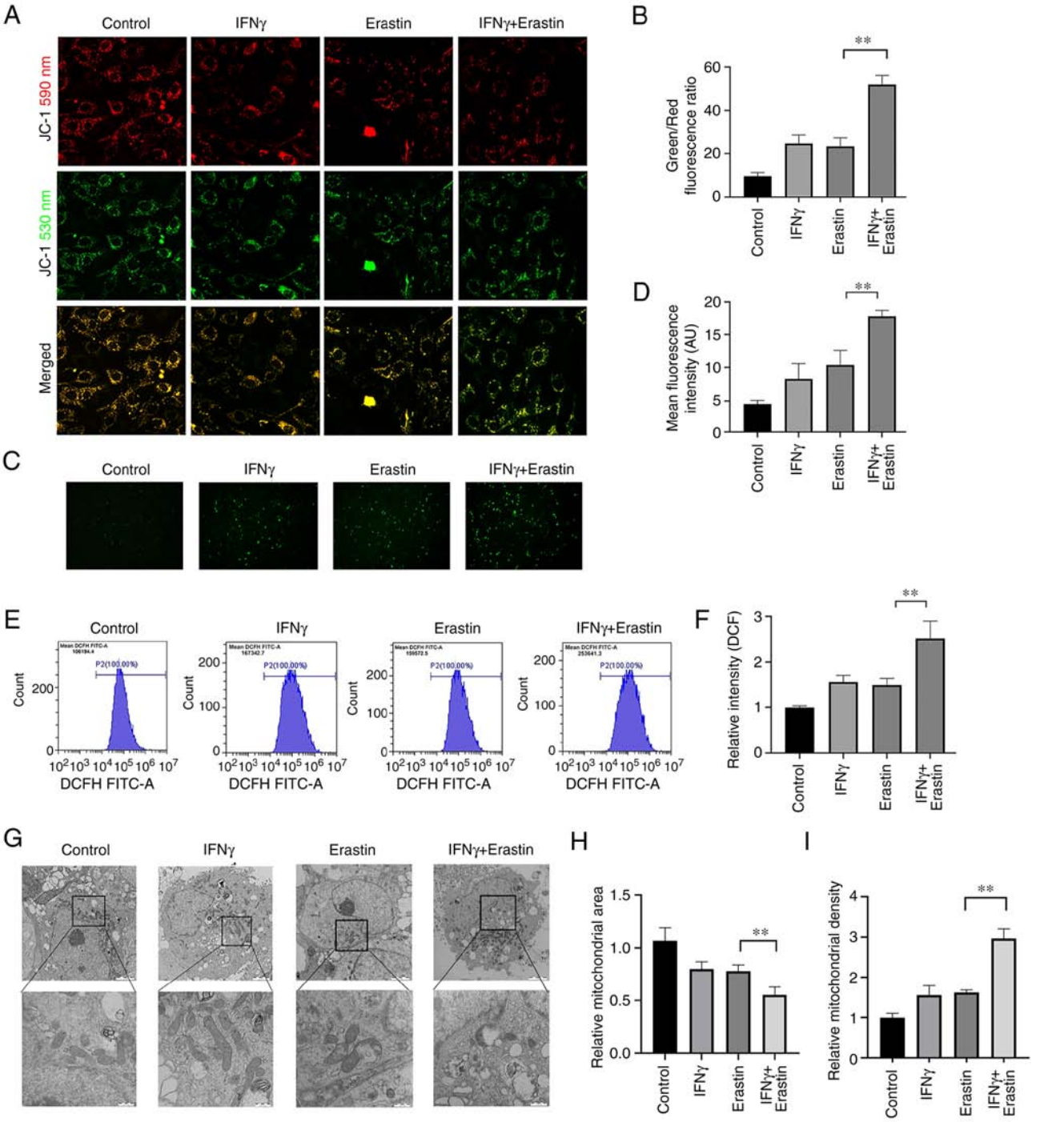

Figure 4. Mitochondrial damage caused by erastin-induced ferroptosis is enhanced by IFNγ. (A) The mitochondrial membrane potential in NCI-H295R cells was observed using confocal fluorescence microscopy (magnification, x400). (B) Bar graph presenting the green/red fluorescence ratio, which reflects the changes in the mitochondrial membrane potential (C) Representative images and (D) quantitative analysis of reactive oxidative stress observed by confocal fluorescence microscopy. (E) Reactive oxygen species production was determined by DCF dihydro-diacetate and analyzed by flow cytometry; (F) a bar graph presenting quantitative results is provided. (G) Morphological changes of mitochondria were observed by transmission electron microscopy. Scale bars, 2 μm for the first row; 0.5 μm for the magnified images; (H and I) the area and density of mitochondria were quantitatively analyzed by using ImageJ software. Values are expressed as the mean ± standard deviation (**P<0.01). DCF, dichlorofluorescein.

IFNγ represses SLC7A11 expression through the JAK/STAT pathway. SLC7A11 has a critical role in ferroptosis. The results of the western blot analysis suggested that the levels of SLC7A11 expression were reduced in erastin-treated NCI-H295R cells. Pretreatment with IFNγ further enhanced the inhibitory effect of erastin on SLC7A11 expression in NCI-H295R cells (Fig. 5A and B). Similar results were also confirmed by RT-qPCR and immunofluorescence analysis (Fig. 5C-E). IFNγ was able to activate the JAK/STAT signaling pathway and mediate immune function and proliferation of cells. It has been demonstrated that STAT3 reduces the expression of SLC7A11 through binding to the promoter of SLC7A11 (26). To further explore the molecular mechanism of the effect of IFNγ to repress SLC7A11 expression, the levels

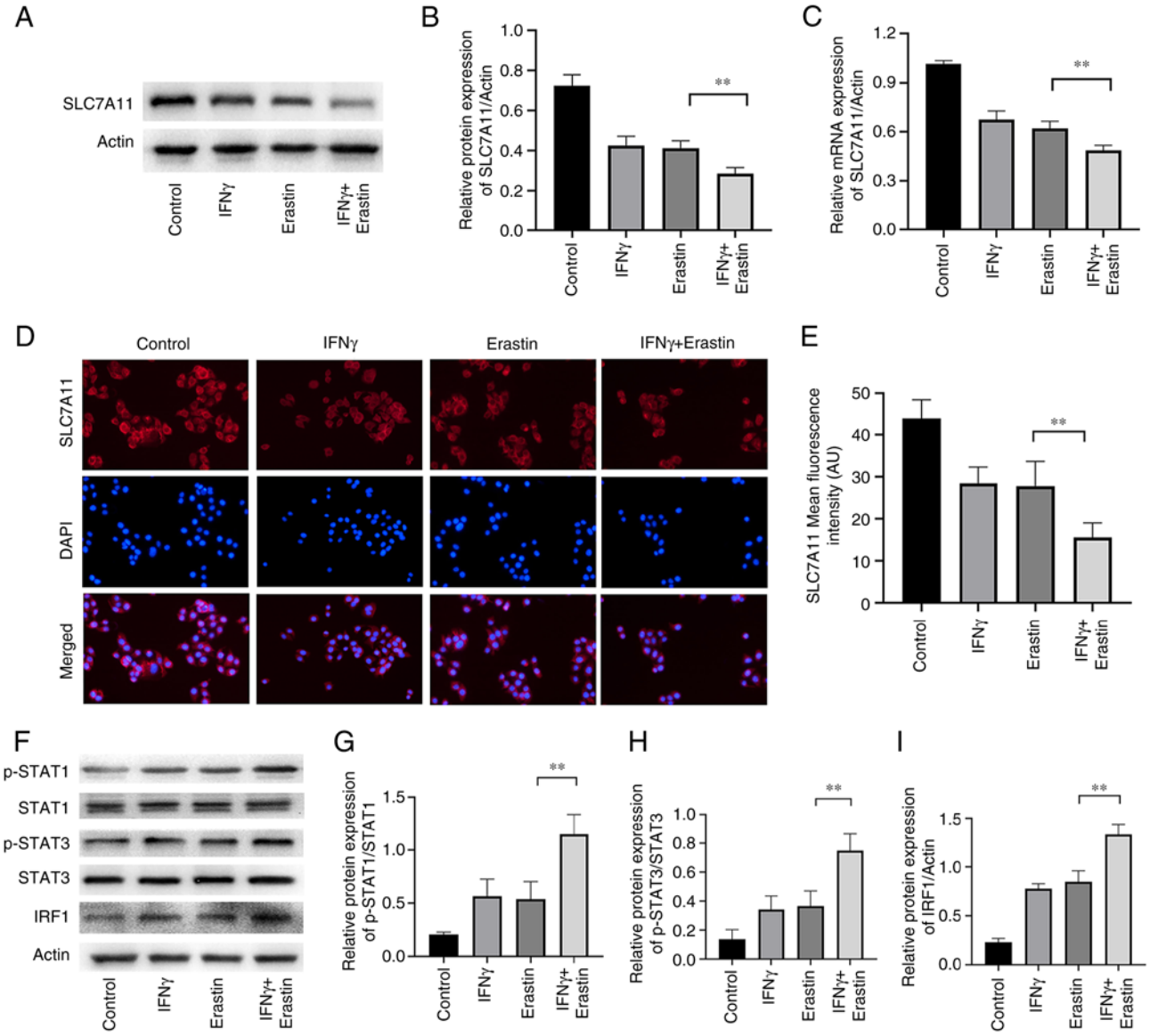

Figure 5. IFNγ represses SLC7A11 expression through the JAK/STAT pathway. (A) Representative western blots of SLC7A11 in NCI-H295R cells and (B) quantified results. (C) Reverse transcription-quantitative PCR analysis was performed to measure the mRNA expression of SLC7A11. (D) Representative images of immunofluorescence observed by confocal fluorescence microscopy, which confirm the expression of SLC7A11, and (E) quantification of the results. (F) Representative western blots and quantification of the results for (G) p-STAT1/STAT1, (H) p-STAT3/STAT3 and (I) IRF1. Values are expressed as the mean ± standard deviation (**P<0.01). SLC7A11, solute carrier family 7 member 11; p-STAT1, phosphorylated signal transducer and activator of transcription; IRF1, IFN regulatory factor 1.

of pSTAT1, pSTAT3 and IRF1 were determined. The results indicated that erastin increased the expression of pSTAT1, pSTAT3 and IRF1, which were further increased by IFNγ in NCI-H295R cells (Fig. 5F-I), suggesting that IFNγ may repress SLC7A11 expression through JAK/STAT pathway.

SLC7A11 overexpression or STAT1 inhibition ameliorates IFNγ-enhanced erastin-induced ferroptosis. Next, it was determined whether IFN-γ was able to promote ferroptosis through repressing SLC7A11 via the JAK/STAT pathway. A plasmid was used to overexpress SLC7A11 and fludarabine was used to inhibit STAT1. The expression levels of SLC7A11 at the mRNA and protein levels were significantly higher in cells transfected with the plasmid compared with the empty vector control (Fig. 6A and B). Cell death was increased in cells transfected with the mock plasmid (Fig. 6C and D). The level of lipid peroxidation and iron accumulation was reduced in SLC7A11-overexpressing NCI-H295R cells and fludarabine-treated NCI-H295R cells (Fig. 6E-H). Furthermore, SLC7A11 overexpression prevented mitochondrial damage in the cells, and STAT1 inhibition exerted a similar effect, although it was weaker (Fig. 6I-K). These results indicated that SLC7A11 inhibited IFNγ-enhanced erastin-induced ferroptosis, and STAT1 aggravated this effect.

Discussion

ACC has a poor prognosis, with a 5-year survival rate of 15% in patients with advanced-stage disease (20). Although the use of immunotherapy for the management of malignant neoplasms has increased, the immunotherapeutic efficacy in ACC is limited owing to the intrinsic mechanisms of

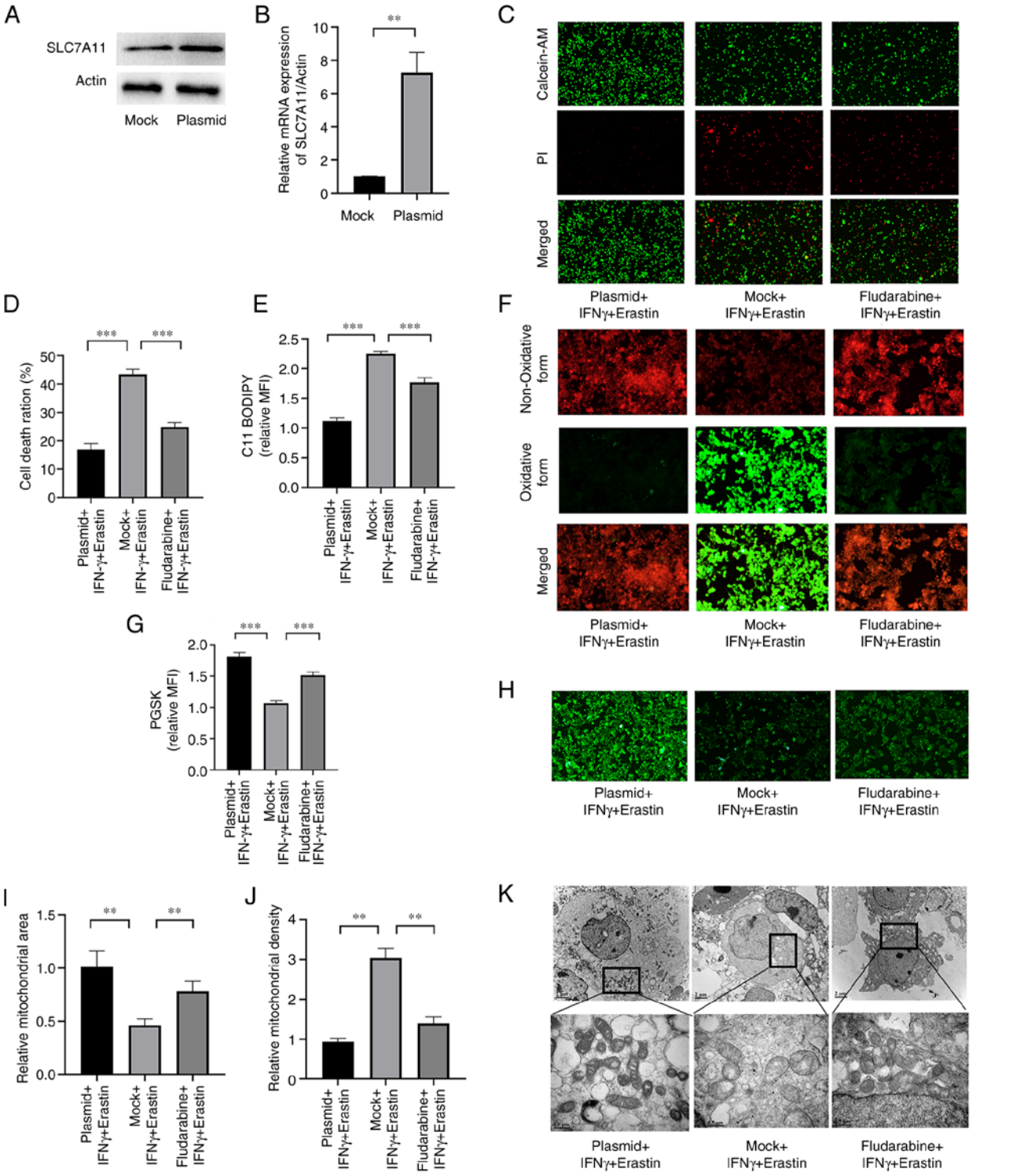

Figure 6. SLC7A11 overexpression or STAT1 suppression ameliorate IFNγ-enhanced erastin-induced ferroptosis. (A) Western blot analysis of SLC7A11 in mock and plasmid groups. (B) Reverse transcription-quantitative PCR analysis was performed to measure the mRNA expression of SLC7A11 in the mock and plasmid groups. (C) Representative images of the Live/Dead cell analysis and (D) quantification of the results. (E) Quantitative results for C11-BODIPY fluorescence and (F) representative images (magnification, x200). (G) Quantitative PGSK fluorescence and (H) representative images (magnification, x100). (I) Mitochondrial area and (J) mitochondrial density determined from transmission electron microscopy images by using the ImageJ software; (K) representative transmission electron microscopy images. Scale bars, 2 μm for the first row; 0.5 μm for the magnified images. Values are expressed as the mean ± standard deviation (**P<0.01 and ***P<0.001). PGSK, Phen Green SK; MFI, mean fluorescence intensity; PI, propidium iodide; AM, acetoxymethyl ester; SLC7A11, solute carrier family 7 member 11.

immunoresistance. Ferroptosis has an important role in affecting the efficacy of cancer immunotherapy (27). It is well established that ferroptosis inducers exert anti-tumor effects in various types of cancer (28). In the present study, the effect of

IFNγ on the sensitivity of the ACC cell line NCI-H295R to a ferroptosis inducer, erastin, was determined.

The differentially expressed FRGs between normal adrenal glands and ACC samples were determined, and univariate Cox regression analysis was then performed to identify prognostic genes (ACSL4, FANCD2, PTGS2, SLC7A11, AIFM2, PGD and ACSF2). Recent research has revealed that a combination of IFNγ derived from immunotherapy-activated $CD8^+$ T cells and radiotherapy-activated ATM promote cancer ferroptosis via synergistic repression of SLC7A11 (29). Thus, it was speculated that SLC7A11 was a novel common gene involved in both ferroptosis and cancer immunotherapy. SLC7A11, an important subunit of cystine/glutamate antiporter system Xc-, mediates cystine uptake and GSH biosynthesis, resulting in the suppression of ferroptosis and reducing oxidative stress (30). Several studies have indicated that SLC7A11 expression is upregulated in various types of cancer (31-33). Weigand *et al* (34) reported that SLC7A11 was upregulated in 33ACC tissues compared with 10 normal adrenal gland samples from the Gene Expression Omnibus dataset GSE10927. Furthermore, the present study determined that SLC7A11 was upregulated in 79 ACC tissues compared with 128 normal adrenal gland tissues based on the TCGA dataset and GTEx dataset. Chen *et al* (35) determined SLC7A11 was correlated with OS of patients with ACC from the TCGA dataset. Shi *et al* (36) reported that high expression of SLC7A11 was significantly associated with a shortened OS in patients with ACC according to the GEPIA2 database; thus, SLC7A11 is a candidate prognostic biomarker for ACC. The present study also indicated that SLC7A11 is a prognosis-related ferroptosis gene in patients with ACC and further explored relevant regulatory mechanisms of SLC7A11 in the ferroptosis of ACC cells. The present study suggested that targeting SLC7A11 was able to promote ferroptosis in ACC cells through IFNγ. Therefore, SLC7A11 may be considered a potential immunological therapeutic target in ACC.

Erastin is a classical ferroptosis inducer that inhibits the activity of System Xc-, thereby facilitating an increase in sensitivity to ferroptosis in tumor cells (37). Erastin has excellent prospects for clinical use, enhancing the sensitivity of various types of human cancer to chemotherapy or radiotherapy (18,19,38). Weigand *et al* (34) demonstrated that ACC cells were insensitive to treatment with Erastin for 24 h. However, recent research suggested that knockdown of SLC7A11 or IFNγ-mediated downregulation of SLC7A11 increased the sensitivity of tumor cells to Erastin-induced ferroptosis (11). Therefore, it was hypothesized that there exists crosstalk between IFNγ-mediated signaling and ferroptosis in ACC. In the present study, it was indicated that pretreatment with IFNγ prolonged the period of action of erastin to inhibit the viability of the NCI-H295R ACC cells.

Ferroptosis is characterized by iron-dependent lipid peroxidation and ROS production. A higher level of ROS generation promotes cancer suppression (39,40). The results of the present study suggested that IFNγ together with erastin enhanced the ferroptosis-like changes, including accumulation of intracellular iron content, elevated levels of lipid peroxidation, increased ROS production and mitochondrial damage. Both GPX4 and ACSL4 are essential determinants of sensitivity to ferroptosis. ACSL4 is involved in the formation of lipid ROS, which leads to ferroptosis, whereas GPX4, using GSH as a substrate, protects cells from lipid peroxidation (15). The results of the present study indicated that the expression of ACSL4 was upregulated in the IFNγ + erastin group, whereas the expression of GPX4 was downregulated. To summarize, these results suggested that IFNγ enhanced erastin-induced ferroptosis in an ACC cell line, highlighting a potential therapeutic approach for the management of ACC.

Pro-inflammatory cytokines, such as IFNγ, are released from immune cells and are responsible for anti-tumor immunity. IFNγ binds to specific receptors at the cell membrane to trigger the phosphorylation of STAT1 and activation of IRF1. This results in the activation of the JAK/STAT signaling pathway, which is an essential signaling pathway involved in regulating SLC7A11 expression (11,12). Recent research confirmed that IFNγ promoted STAT1-mediated suppression of SLC7A11 in HT-1080 cells (11). In addition, STAT3 and STAT5 contribute to the regulation of SLC7A11 in numerous types of cancer, such as breast cancer (41). The results of the present study suggested that dual treatment with IFNγ and erastin significantly suppressed the expression of SLC7A11. Furthermore, IFNγ treatment indirectly upregulated the expression of pSTAT1, pSTAT3 and IRF1. In addition, SLC7A11 overexpression or STAT1 inhibition significantly ameliorated IFNγ-enhanced erastin-induced ferroptosis. Therefore, it may be hypothesized that IFNγ inhibits SLC7A11 via the JAK/STAT pathway.

The present study has certain limitations. First, ferroptosis-inhibiting drugs, such as ferrostatin-1, were not used to explore their protective effects under IFNγ-enhanced erastin-induced ferroptosis. Furthermore, the role of IFNγ was not verified *in vivo* or in another ACC cell line. In addition, a comparison of the expression status of SLC7A11 between normal adrenocortical cells and NCI-H295R was not performed due to the lack of normal adrenocortical cells. The above-mentioned factors will be investigated in future studies.

In conclusion, it was demonstrated for the first time that IFNγ treatment increased the sensitivity of ACC cells to erastin-induced ferroptosis via downregulation of SLC7A11 via the JAK/STAT pathway. Furthermore, it increased the levels of lipid peroxidation and ROS and increased mitochondrial damage, which in turn led to ferroptosis in ACC tumor cells. The present study provides critical insight into ferroptosis and how it may be used to improve the efficacy of cancer immunotherapy in ACC.

Acknowledgements

The authors express their gratitude to Dr Lei Guo (Department of Orthopaedics, Ruijin Hospital, Shanghai Jiao Tong University School of Medicine, Shanghai, China) for providing experimental assistance for this research.

Funding

This work was supported by the Natural Science Foundation of Shanghai, China (grant no. 21ZR1440700).

Availability of data and materials

All data generated and/or analyzed during the present study are included in this published article.

Authors' contributions

XY and DZ contributed to the design of the study, performed the study and wrote the manuscript. BL contributed to the statistical analysis of the data. WK and YC contributed to cell culture. YZ analyzed the data and edited the manuscript. All authors contributed to the article, and read and approved the final version. XY and YZ confirm the authenticity of all the raw data.

Ethics approval and consent to participate

Not applicable.

Patient consent for publication

Not applicable.

Competing interests

The authors declare that they have no competing interests.

References

1. Assié G, Letouzé E, Fassnacht M, Jouinot A, Luscap W, Barreau O, Omeiri H, Rodriguez S, Perlemoine K, René-Corail F, *et al*: Integrated genomic characterization of adrenocortical carcinoma. Nat Genet 46: 607-612, 2014.
2. Crona J and Beuschlein F: Adrenocortical carcinoma-towards genomics guided clinical care. Nat Rev Endocrinol 15: 548-560, 2019.
3. Le Tourneau C, Hoimes C, Zarwan C, Wong DJ, Bauer S, Claus R, Wermke M, Hariharan S, von Heydebreck A, Kasturi V, *et al*: Avelumab in patients with previously treated metastatic adrenocortical carcinoma: phase 1b results from the JAVELIN solid tumor trial. J Immunother Cancer 6: 111, 2018.
4. Sperone P, Ferrero A, Daffara F, Priola A, Zaggia B, Volante M, Santini D, Vincenzi B, Badalamenti G, Intrivici C, *et al*: Gemcitabine plus metronomic 5-fluorouracil or capecitabine as a second-/third-line chemotherapy in advanced adrenocortical carcinoma: A multicenter phase II study. Endocr Relat Cancer 17: 445-453, 2010.
5. Henning JEK, Deutschbein T, Altieri B, Steinhauer S, Kircher S, Sbiera S, Wild V, Schlötelburg W, Kroiss M, Perotti P, *et al*: Gemcitabine-based chemotherapy in adrenocortical carcinoma: A multicenter study of efficacy and predictive factors. J Clin Endocrinol Metab 102: 4323-4332, 2017.
6. Cosentini D, Grisanti S, Dalla Volta A, Laganà M, Fiorentini C, Perotti P, Sigala S and Berruti A: Immunotherapy failure in adrenocortical cancer: Where next? Endocr Connect 7: E5-E8, 2018.
7. Jorgovanovic D, Song M, Wang L and Zhang Y: Roles of IFN-γ in tumor progression and regression: A review. Biomark Res 8: 49, 2020.
8. Ni L and Lu J: Interferon gamma in cancer immunotherapy. Cancer Med 7: 4509-4516, 2018.
9. Ligocki AJ, Brown JR and Niederkorn JY: Role of interferon-γ and cytotoxic T lymphocytes in intraocular tumor rejection. J Leukoc Biol 99: 735-747, 2016.
10. Zhou J, Ma P, Li J, Cui X and Song W: Improvement of the cytotoxic T lymphocyte response against hepatocellular carcinoma by transduction of cancer cells with an adeno-associated virus carrying the interferon-γ gene. Mol Med Rep 13: 3197-3205, 2016.
11. Wang W, Green M, Choi JE, Gijon M, Kennedy PD, Johnson JK, Liao P, Lang X, Kryczek I, Sell A, *et al*: CD8(+) T cells regulate tumour ferroptosis during cancer immunotherapy. Nature 569: 270-274, 2019.
12. Kong R, Wang N, Han W, Bao W and Lu J: IFNγ-mediated repression of system xc^- drives vulnerability to induced ferroptosis in hepatocellular carcinoma cells. J Leukoc Biol 110: 301-314, 2021.
13. Mou Y, Wang J, Wu J, He D, Zhang C, Duan C and Li B: Ferroptosis, a new form of cell death: Opportunities and challenges in cancer. J Hematol Oncol 12: 34, 2019.
14. Zhang X and Li X: Abnormal iron and lipid metabolism mediated ferroptosis in kidney diseases and its therapeutic potential. Metabolites 12: 58, 2022.
15. Li D and Li Y: The interaction between ferroptosis and lipid metabolism in cancer. Signal Transduct Target Ther 5: 108, 2020.
16. Tang X, Chen W, Liu H, Liu N, Chen D, Tian D and Wang J: Research progress on SLC7A11 in the regulation of cystine/cysteine metabolism in tumors. Oncol Lett 23: 47, 2022.
17. Wang Y, Wei Z, Pan K, Li J and Chen Q: The function and mechanism of ferroptosis in cancer. Apoptosis 25: 786-798, 2020.
18. Cobler L, Zhang H, Suri P, Park C and Timmerman L: xCT inhibition sensitizes tumors to γ-radiation via glutathione reduction. Oncotarget 9: 32280-32297, 2018.
19. Chen L, Li X, Liu L, Yu B, Xue Y and Liu Y: Erastin sensitizes glioblastoma cells to temozolomide by restraining xCT and cystathionine-γ-lyase function. Oncol Rep 33: 1465-1474, 2015.
20. Roh JL, Kim EH, Jang HJ, Park JY and Shin D: Induction of ferroptotic cell death for overcoming cisplatin resistance of head and neck cancer. Cancer Lett 381: 96-103, 2016.
21. Liang JY, Wang DS, Lin HC, Chen XX, Yang H, Zheng Y and Li YH: A novel ferroptosis-related gene signature for overall survival prediction in patients with hepatocellular carcinoma. Int J Biol Sci 16: 2430-2441, 2020.
22. Team C: Team RDC.R: A Language And Environment For Statistical Computing. R Foundation for Statistical Computing, Vienna, 2012.
23. Ritchie ME, Phipson B, Wu D, Hu Y, Law CW, Shi W and Smyth GK: Limma powers differential expression analyses for RNA-sequencing and microarray studies. Nucleic Acids Res 43: e47, 2015.
24. Tang Z, Li C, Kang B, Gao G, Li C and Zhang Z: GEPIA: A web server for cancer and normal gene expression profiling and interactive analyses. Nucleic Acids Res 45: W98-W102, 2017.
25. Livak KJ and Schmittgen TD: Analysis of relative gene expression data using real-time quantitative PCR and the 2(-Delta Delta C(T)) Method. Methods 25: 402-408, 2001.
26. Linher-Melville K, Haftchenary S, Gunning P and Singh G: Signal transducer and activator of transcription 3 and 5 regulate system Xc- and redox balance in human breast cancer cells. Mol Cell Biochem 405: 205-221, 2015.
27. Sun L, Linghu D and Hung M: Ferroptosis: A promising target for cancer immunotherapy. Am J Cancer Res 11: 5856-5863, 2021.
28. Xia X, Fan X, Zhao M and Zhu P: The Relationship between ferroptosis and tumors: A novel landscape for therapeutic approach. Curr Gene Ther 19: 117-124, 2019.
29. Lang X, Green MD, Wang W, Yu J, Choi JE, Jiang L, Liao P, Zhou J, Zhang Q, Dow A, *et al*: Radiotherapy and immunotherapy promote tumoral lipid oxidation and ferroptosis via synergistic repression of SLC7A11. Cancer Discov 9: 1673-1685, 2019.
30. Koppula P, Zhuang L and Gan B: Cystine transporter SLC7A11/xCT in cancer: Ferroptosis, nutrient dependency, and cancer therapy. Protein Cell 12: 599-620, 2021.
31. Jiang L, Kon N, Li T, Wang SJ, Su T, Hibshoosh H, Baer R and Gu W: Ferroptosis as a p53-mediated activity during tumour suppression. Nature 520: 57-62, 2015.
32. Shiozaki A, Iitaka D, Ichikawa D, Nakashima S, Fujiwara H, Okamoto K, Kubota T, Komatsu S, Kosuga T, Takeshita H, *et al*: xCT, component of cysteine/glutamate transporter, as an independent prognostic factor in human esophageal squamous cell carcinoma. J Gastroenterol 49: 853-863, 2014.
33. Takeuchi S, Wada K, Toyooka T, Shinomiya N, Shimazaki H, Nakanishi K, Nagatani K, Otani N, Osada H, Uozumi Y, *et al*: Increased xCT expression correlates with tumor invasion and outcome in patients with glioblastomas. Neurosurgery 72: 33-41; discussion 41, 2013.
34. Weigand I, Schreiner J, Rohrig F, Sun N, Landwehr LS, Urlaub H, Kendl S, Kiseljak-Vassiliades K, Wierman ME, Angeli JPF, *et al*: Active steroid hormone synthesis renders adrenocortical cells highly susceptible to type II ferroptosis induction. Cell Death Dis 11: 192, 2020.
35. Chen X, Yan L, Jiang F, Lu Y, Zeng N, Yang S and Ma X: Identification of a ferroptosis-related signature associated with prognosis and immune infiltration in adrenocortical carcinoma. Int J Endocrinol 2021: 4654302, 2021.

36. Shi Z, Tao H, Fan Z, Song S and Bai J: Prognostic and immunological role of key genes of ferroptosis in pan-cancer. Front Cell Dev Biol 9: 748925, 2021.
37. Tang R, Xu J, Zhang B, Liu J, Liang C, Hua J, Meng Q, Yu X and Shi S: Ferroptosis, necroptosis, and pyroptosis in anticancer immunity. J Hematol Oncol 13: 110, 2020.
38. Yamaguchi H, Hsu JL, Chen CT, Wang YN, Hsu MC, Chang SS, Du Y, Ko HW, Herbst R and Hung MC: Caspase-independent cell death is involved in the negative effect of EGF receptor inhibitors on cisplatin in non-small cell lung cancer cells. Clin Cancer Res 19: 845-854, 2013.
39. Belavgeni A, Bornstein SR, von Mässenhausen A, Tonnus W, Stumpf J, Meyer C, Othmar E, Latk M, Kanczkowski W, Kroiss M, *et al*: Exquisite sensitivity of adrenocortical carcinomas to induction of ferroptosis. Proc Natl Acad Sci USA 116: 22269-22274, 2019.
40. Wu S, Li T, Liu W and Huang Y: Ferroptosis and cancer: Complex relationship and potential application of exosomes. Front Cell Dev Biol 9: 733751, 2021.
41. Linher-Melville K and Singh G: The complex roles of STAT3 and STAT5 in maintaining redox balance: Lessons from STAT-mediated xCT expression in cancer cells. Mol Cell Endocrinol 451: 40-52, 2017.